ECS The Electrochemical Society
Advancing solid state & electrochemical science & technology

Tailoring the Ag$^+$ Content within the Tunnels and on the Exposed Surfaces of α-MnO$_2$ Nanowires: Impact on Impedance and Electrochemistry

View the article online for updates and enhancements.

Tailoring the Ag$^+$ Content within the Tunnels and on the Exposed Surfaces of α-MnO$_2$ Nanowires: Impact on Impedance and Electrochemistry

Bingjie Zhang,[a] Paul F. Smith,[a] Seung-Yong Lee,[b] Lijun Wu,[b] Yimei Zhu,[b] Esther S. Takeuchi,[a,b,c,*,z] Amy C. Marschilok,[a,c,**,z] and Kenneth J. Takeuchi[a,c,**,z]

[a]*Department of Chemistry, Stony Brook University, Stony Brook, New York 11794, USA*
[b]*Energy Sciences Directorate, Brookhaven National Laboratory, Upton, New York 11973, USA*
[c]*Department of Materials Science and Engineering, Stony Brook University, Stony Brook, New York 11794, USA*

Efficient conduction of both electrons and cations (e.g., Li$^+$) has a profound effect on the current and capacity of lithium-based batteries. With this study, we focus on cathode effects, with the preparation of pure silver hollandite materials with variable silver ion content within (intra-tunnel) and on the surface of α-MnO$_2$ tunneled materials, followed by the measurement and analysis of impedance and electrochemistry data. Specifically, pure Ag$_x$Mn$_8$O$_{16-y}$ materials with low (x = 1.13) and high (x = 1.54) intra-tunnel silver content are compared with Ag$_x$Mn$_8$O$_{16-y}$ · aAg$_2$O (a = 0.25, 0.63, 1.43) composites prepared via a new Ag$_2$O coating strategy. When the Ag$_2$O (a = 0, 0.25) content is low, the material with higher intra-tunnel silver (x = 1.53) content delivers up to ∼5-fold higher capacity accounted for by a ∼10-fold lower impedance than its lower intra-tunnel silver (x = 1.13) counterpart. In the presence of high Ag$_2$O content (a = 0.63, 1.43), both composites exhibit comparable impedance but the lower intra-tunnel silver (x = 1.13) composite delivers up to ∼1.5-fold higher capacity than higher intra-tunnel silver composite, highlighting the key role of Li$^+$ transport under those conditions. Our results demonstrate material design strategies which can significantly increase electronic and ionic conductivities.

Manganese oxide based materials are the subject of a number of electrochemical studies associated with electrical energy storage applications due in part to their relatively low cost and high theoretical capacity. In particular, α-MnO$_2$ (hollandite or cryptomelane), has corner- and edge-sharing MnO$_6$ octahedra which interlink to form square tunnels consisting of 2 octahedra × 2 octahedra with 0.46 nm diameters.[1–4] Mono or divalent cations often partially occupy the tunnel interior leading to manganese being mixed valent Mn$^{3+/4+}$.[5–7] A member of this class of materials, silver hollandite (Ag$_x$Mn$_8$O$_{16}$)[8] has found application as a sorbent and catalyst under a wide array of applications.[9–12] Silver hollandite is conceptually appealing as a battery cathode because the Ag$^+$ center provides the opportunity to be electrochemically active and reduce to Ag^0 in-situ.[13] Further, if the Ag$^+$ within the tunnel is not electrochemically active, it can provide internal structural support to the tunnel. The synthesis and electrochemical properties of pure silver hollandite have been reported where the material can deliver a capacity of >180 mAh/g.[14,15]

Successful cathode materials for secondary lithium battery applications demand high power output and long-term cycle stability.[16] In order to achieve this, facile transport of both lithium ions and electrons is needed. A strategy that has been used to address one or both of these issues is to surface coat the electroactive cathode materials, as coatings can successfully provide a number of important functions. As an example of a protective mechanism, Al$_2$O$_3$ coated Li$_2$MnO$_3$ exhibited improved specific discharge capacity, cycling stability, and mitigated charge transfer impedance when compared to LiMnO$_2$;[17] Al$_2$O$_3$ coated Li[Li$_{0.20}$Mn$_{0.54}$Ni$_{0.13}$Co$_{0.13}$]O$_2$ showed improved capacity retention of ∼98% after 32 cycles compared to ∼77% retention in the pure materials.[18]

Coatings can also serve to improve electronic conductivity. For example, carbon coatings of active materials have been used for battery relevant materials.[19–22] The conductivity of carbon can be affected by a variety of factors, including physical dimensions, purity and directionality, and is typically in a range of 3.3 × 10^2 to 3 × 10^5 S/m.[23] Ag metal is an excellent electrical conductor with a conductivity of 6.30 × 10^7 S/m.[23] Due to the rarity of Ag, Ag$_2$O is typically surface deposited in small amounts, where the surface of the target material is decorated with small spheres of Ag$_2$O, forming a composite. For example, composites of Cr$_2$O$_3$-Ag$_2$O were prepared which showed higher capacity and capacity retention compared to that of Cr$_2$O$_3$ (641 mAh/g);[24] Further, the composite CuCrO$_2$-Ag$_2$O exhibited a resistance of 63 Ω after discharge (Ag$^+$ + e- → Ag^0) compared to 344 Ω for CuCrO$_2$, highlighting the improved conductivity due to the Ag^0 deposits on the surface of CuCrO$_2$.

In addition to the effects of Ag$_2$O deposited on the surface of electroactive materials to generate composites, the formation of Ag^0 metal during the electrochemical reduction of structural Ag$^+$ (Ag$^+$ contained within the crystal lattice) was confirmed in the case of silver vanadium phosphorus oxide (Ag$_2$VO$_2$PO$_4$). For Ag$_2$VO$_2$PO$_4$, the two Ag$^+$ are contained within the VO$_2$PO$_4^{2-}$ lattice,[25] but Ag^0 is observed as small deposits on the particle surfaces and detected by X-ray diffraction. Notably, upon Ag^0 formation, a reduction in impedance of ∼15000 fold compared to the original material is observed.[26]

For tunneled manganese oxides (α-MnO$_2$), a variety of cations can be observed within the tunnels, including Ag$^+$, yielding materials of the general formula Ag$_x$Mn$_8$O$_{16-y}$. Specifically, we reported that Ag$_{1.16}$Mn$_8$O$_{14.8}$ exhibit a 7-fold increase in discharge capacity relative to Ag$_{1.63}$Mn$_8$O$_{15.6}$, due largely to the oxygen deficiencies associated with Ag$_{1.16}$Mn$_8$O$_{14.8}$.[27] To examine a possible role of Ag$^+$ in the electrochemistry of Ag$_x$Mn$_8$O$_{16-y}$, we developed a Ag$_2$O precipitation strategy to prepare Ag$_x$Mn$_8$O$_{16-y}$ · aAg$_2$O composites for the first time, providing variable amounts of Ag$_2$O spherical deposits on the Ag$_x$Mn$_8$O$_{16-y}$ nanorod surface. Herein, we report the syntheses of the composites and the characterization, including X-ray diffraction

*Electrochemical Society Fellow.
**Electrochemical Society Member.
zE-mail: esther.takeuchi@stonybrook.edu; amy.marschilok@stonybrook.edu; kenneth.takeuchi.1@stonybrook.edu

(XRD), thermogravimetric analysis (TGA), Fourier transform infrared spectroscopy (FTIR) and Transmission electron microscopy (TEM). We also interpret the effects of both the intra-tunnel Ag^+ as well as the Ag_2O surface deposits on the composite electrochemistry using galvanostatic reduction and electrochemical impedance spectroscopy (EIS) measurements.

Experimental

Materials synthesis.—Silver hollandite was prepared via ambient pressure reflux with reagent mixtures containing different Ag/Mn ratios using a method previously reported.[13,15] The abbreviation $Ag_xMn_8O_{16-y}$, where x = Ag content, is used here for simplicity. Ag_2O coated $Ag_xMn_8O_{16-y}$ was synthesized via a coprecipitation reaction as follows. The above synthesized $Ag_xMn_8O_{16-y}$ powder was added to a N_2 degassed $AgNO_3$ solution at 0°C with vigorous stirring to obtain a suspension. A solution of NaOH was added to the $Ag_xMn_8O_{16-y}$ suspension. Three different molar ratios, 2:1, 1:1 and 1:2 of $Ag_xMn_8O_{16-y}$ to Ag_2O were prepared with 1:1, 1:2 and 1:4 molar ratios of $Ag_xMn_8O_{16-y}$ to $AgNO_3$. The abbreviation $Ag_{1.13}Mn_8O_{16-y} \cdot aAg_2O$ is used for simplicity. After chemical precipitation, the as-prepared samples were washed with DI water and dried in vacuo. Pure Ag_2O was also synthesized using the same method without adding silver hollandite.

Materials characterization.—Powder X-ray diffraction (XRD) was employed to characterize the crystal structure and estimate crystallite sizes. The XRD patterns were measured using a Rigaku Smart Lab X-ray diffractometer with Cu Kα radiation and Bragg−Brentano focusing geometry. An MDI JADE version 8.5.3 software with ICDD and NIST databases was used for search-match analysis. A TA Instruments SDT Q600 was used to collect simultaneous thermogravimetric analysis/differential scanning calorimetry (TGA/DSC) for determination of oxygen content of silver hollandite samples according

Table I. Densities of the pellet electrodes.

Compound Stoichiometry $Ag_xMn_8O_{16-y} \cdot aAg_2O$	Pellet density (g/cm^3)
$Ag_{1.13}Mn_8O_{15.15}$	2.36
$Ag_{1.13}Mn_8O_{15.15} \cdot 0.25Ag_2O$	2.66
$Ag_{1.13}Mn_8O_{15.15} \cdot 0.63Ag_2O$	2.51
$Ag_{1.13}Mn_8O_{15.15} \cdot 1.43Ag_2O$	2.64
$Ag_{1.54}Mn_8O_{15.48}$	2.35
$Ag_{1.54}Mn_8O_{15.48} \cdot 0.25Ag_2O$	2.71
$Ag_{1.54}Mn_8O_{15.48} \cdot 0.63Ag_2O$	2.61
$Ag_{1.54}Mn_8O_{15.48} \cdot 1.43Ag_2O$	2.40

to the method previously described.[27] A Thermo Scientific Nicolet iS10 spectrophotometer with attenuated total reflectance accessory (ATR) was applied in the wave number range from 4000 cm^{-1} to 500 cm^{-1} for FT-IR. A Thermo Scientific ICAP 6300 radial inductively coupled plasma optical emission spectrometer (ICP-OES) was used for the quantitative Ag and Mn determination. Transmission electron microscopy (TEM) data was collected by a transmission electron microscope (JEOL JEM 1400) equipped with a Gatan CCD camera.

The ratios of $Ag_xMn_8O_{16-y}$ to Ag_2O were determined using the following method. First, the Ag/Mn ratio of the parent silver hollandite was determined. Then, the total Ag (from both hollandite and silver oxide) and Mn amounts were determined for the coated materials. The value of a in $Ag_xMn_8O_{16-y} \cdot aAg_2O$ was then calculated according to the silver amount in hollandite and in silver oxide.

Electrochemical testing.—Electrodes were prepared by pressing pellets of the as-synthesized materials and the densities of the pellet electrodes are shown in Table I. Coin type cells were fabricated within an argon glove box with lithium metal anodes and 1 M $LiPF_6$ in 70/30 (V/V) dimethyl carbonate/ethylene carbonate electrolyte.
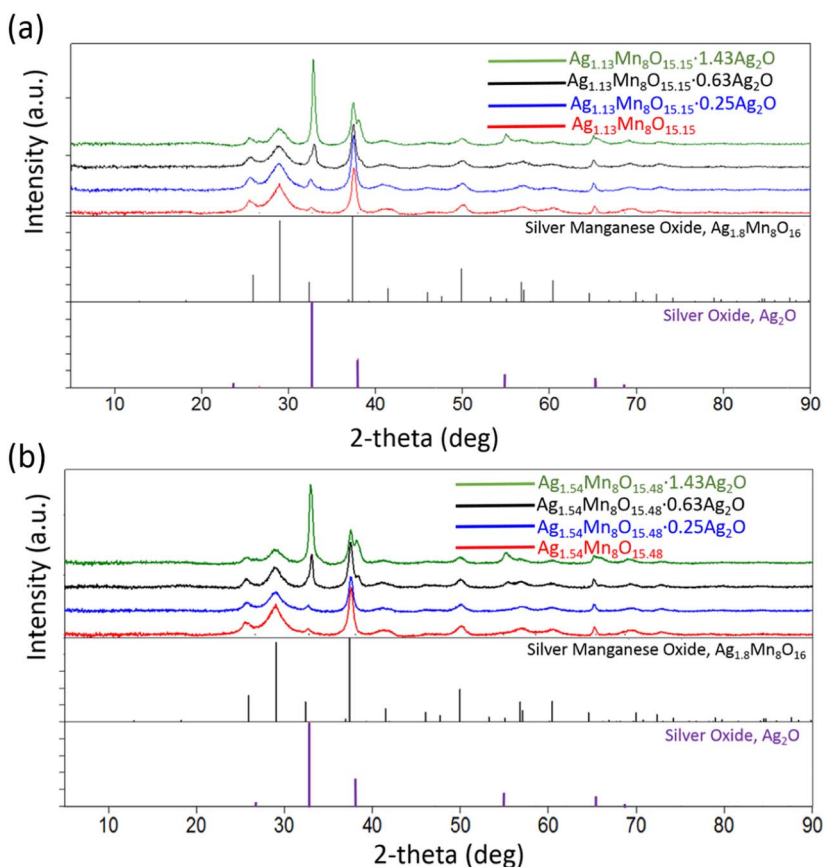
Figure 1. XRD patterns of (a) $Ag_{1.13}Mn_8O_{15.15}$ and (b) $Ag_{1.54}Mn_8O_{15.48}$ coated with different ratios of Ag_2O.

Table II. Empirical formulas for Ag_2O coated $Ag_xMn_8O_{16-y}$ determined by ICP-OES and TGA.

Reactant Ratio $Ag_xMn_8O_{16-y}$:$AgNO_3$	Product Stoichiometry $Ag_xMn_8O_{16-y} \cdot aAg_2O$
$Ag_{1.13}Mn_8O_{15.15}$:$AgNO_3$ = 1:1	$Ag_{1.13}Mn_8O_{15.15} \cdot 0.25Ag_2O$
$Ag_{1.13}Mn_8O_{15.15}$:$AgNO_3$ = 1:2	$Ag_{1.13}Mn_8O_{15.15} \cdot 0.63Ag_2O$
$Ag_{1.13}Mn_8O_{15.15}$:$AgNO_3$ = 1:4	$Ag_{1.13}Mn_8O_{15.15} \cdot 1.43Ag_2O$
$Ag_{1.54}Mn_8O_{15.48}$:$AgNO_3$ = 1:1	$Ag_{1.54}Mn_8O_{15.48} \cdot 0.25Ag_2O$
$Ag_{1.54}Mn_8O_{15.48}$:$AgNO_3$ = 1:2	$Ag_{1.54}Mn_8O_{15.48} \cdot 0.63Ag_2O$
$Ag_{1.54}Mn_8O_{15.48}$:$AgNO_3$ = 1:4	$Ag_{1.54}Mn_8O_{15.48} \cdot 1.43Ag_2O$

Intermittent discharge with a current density of 1 mA/g was employed. The discharge process was stopped every 1% of theoretical capacity three times and every 5% of theoretical capacity for the remainder of the test. AC impedance measurements were measured after ~12 h at OCV using a BioLogic VSP impedance analyzer with a 10 mV amplitude and a frequency range of 100 kHz to 0.1 Hz. The Nyquist plots were normalized assuming a zero intercept at the high frequency x-axis intercept for comparison of R_{CT}. Equivalent circuit analysis was performed using Z-view software.[16,28]

Results and Discussion

Material characterization.—The XRD patterns of representative as-prepared hollandites are presented in Figure 1, red traces, for low (a) and high (b) silver content. All peaks can be indexed to the reference pattern (JCPDS card No. 97-006-015). The XRD patterns for samples coated with Ag_2O show intense PXRD reflections at 34°, 37° and 56° 2θ, in agreement with cubic Ag_2O, Figure 1, green traces. Samples prepared with lower Ag_2O content gave less intense XRD peaks consistent with the ability to tune the coating amount. For samples with low levels of Ag_2O, XRD could not readily discern the peaks corresponding to the silver oxide phase.[29] The presence of lower amounts of the Ag_2O coating was confirmed by alternate techniques, as described below.

Empirical formulas for all the materials were determined by ICP-OES in conjunction with TGA. Typical as-prepared hollandites resulted in of $Ag_xMn_8O_{16-y}$, x = 1.13 and x = 1.54, for the low silver and high silver materials, respectively. The oxygen contents of y = 15.15 (x = 1.13, low silver) and 15.48 (x = 1.54, high silver) were determined yielding formulas of $Ag_{1.13}Mn_8O_{15.15}$ and $Ag_{1.54}Mn_8O_{15.48}$.[27] The fraction of Ag_2O in the final precipitate was roughly proportional to the $Ag_xMn_8O_{16-y}$: Ag ratio used during synthesis, Table II.

FTIR spectra were recorded for all the samples, Figure 2. Pure Ag_2O demonstrates two main peaks at 1380 and 881 cm^{-1}, consistent with previously published data at 1379 and 901 cm^{-1}.[30] As the Ag_2O/$Ag_{1.13}Mn_8O_{15.15}$ ratio increases, the FTIR spectra continue to demonstrate the silver hollandite peaks, while the peaks detected at ~1380 cm^{-1} increase. The XRD and FTIR data indicate that the silver hollandite structure remains intact throughout the coating procedure[31] with no apparent change of $Ag_{1.13}Mn_8O_{15.15}$ lattice constants despite the presence of Ag_2O.

The presence of a silver rich composition to the nanoparticle coating was confirmed by TEM, Figure 3. As-prepared $Ag_{1.13}Mn_8O_{15.15}$ and $Ag_{1.54}Mn_8O_{15.48}$ (Figures 3a, 3b) are ~15 nm diameter nanorods with smooth surfaces. With increasing Ag_2O content, nanoparticles up to size 5~10 nm are visible on the surface of the nanorods (Figures 3g, 3h). HAADF-STEM and STEM-EDS images confirmed these particles contain mostly silver, Figure S1, suggesting these are the deposited Ag_2O. It can be seen in all images that the deposited nanoparticles are distributed uniformly.

Electrochemical analysis.—Lithium anode electrochemical cells were prepared using Ag_2O, $Ag_xMn_8O_{16-y}$ and the $Ag_xMn_8O_{16-y} \cdot aAg_2O$ composites as cathodes. Electrochemical impedance spectroscopy was used to characterize the cells before and after reduction.
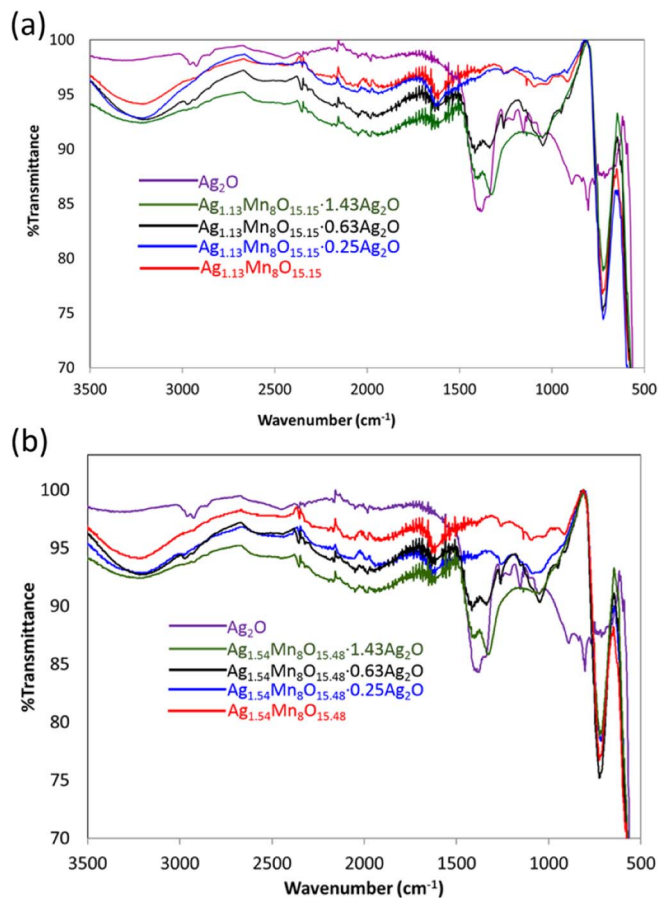

Figure 2. FT-IR of (a) Ag_2O, $Ag_{1.13}Mn_8O_{15.15}$, $Ag_{1.13}Mn_8O_{15.15} \cdot 0.25$ Ag_2O, $Ag_{1.13}Mn_8O_{15.15} \cdot 0.63Ag_2O$ and $Ag_{1.13}Mn_8O_{15.15} \cdot 1.43Ag_2O$ (b) Ag_2O, $Ag_{1.54}Mn_8O_{15.48}$, $Ag_{1.54}Mn_8O_{15.48} \cdot 0.25Ag_2O$, $Ag_{1.54}Mn_8O_{15.48} \cdot 0.63Ag_2O$ and $Ag_{1.54}Mn_8O_{15.48} \cdot 1.43Ag_2O$.

The Nyquist plots of all cells showed a similar characteristic semicircle, Figures 4–8. The data were fitted to an equivalent circuit consisting of a resistor (Rs), a parallel combination of a resistor ($Rct1$) and a constant phase element (CPE), the other parallel combination of a resistor ($Rct2$) and CPE and a Warburg element (open, W_0), Table III.

A pure Ag_2O cathode was characterized as a control. The voltage profile is shown in Figure 4a, where the initial loaded voltage of 2.96 V recovers to 3.1–3.2 V within the first 0.004 molar electron equivalents of reduction. This phenomenon of voltage increase upon reduction has been observed previously in the discharge of $Ag_2VO_2PO_4$ and was attributed to Ag^0 nanoparticle formation,[32] with concomitant decrease in resistance. For the Li/Ag_2O cell, ~1000-fold reduction in impedance was observed upon reduction by 0.02 molar electron equivalents (501 Ω) compared to that before discharge (339560 Ω), Figure 4b. Discharge continues with two voltage plateaus, at ~3.1 V, and 2.2 V until ~0.52 electron equivalents (~65 mAh/g) followed by a steeper decrease. Notably, cell resistance continued decreasing with depth of discharge to a final value of 176 Ω at a voltage of 1.5 V. Above 2.2 V, Ag_2O contribution to capacity (20 mAh/g, 0.17 electron equivalents) is small. For the electrode sample with maximum Ag_2O content ($Ag_{1.54}Mn_8O_{15.48} \cdot 1.43Ag_2O$), a maximum contribution to capacity of 6 mAh/g above 2.2 V can be ascribed to Ag_2O based on mass.
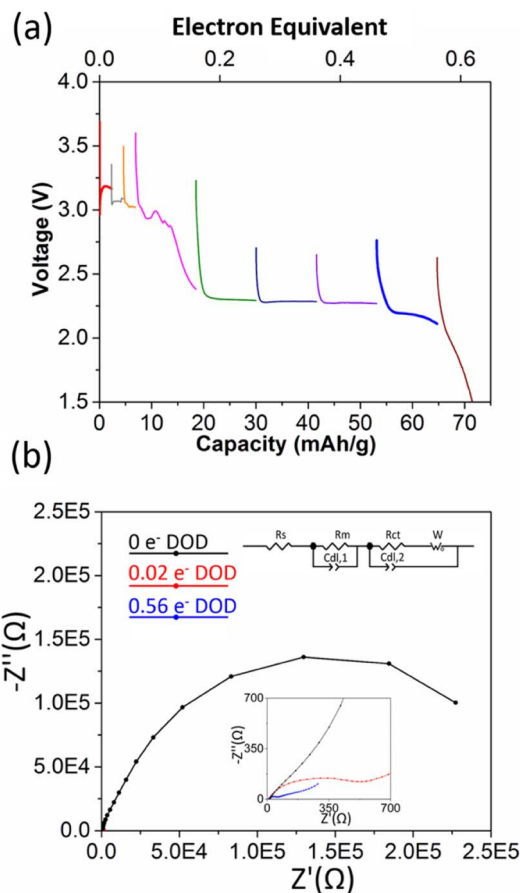
The discharge profiles of pure pellets comprised of only $Ag_{1.13}Mn_8O_{15.15}$ or $Ag_{1.54}Mn_8O_{15.48}$ materials are shown in Figures 5a and 5b, respectively. Both hollandite materials show abrupt decreases in their voltages upon initial reduction. Above 2.2 V, $Ag_{1.13}Mn_8O_{15.15}$ discharges 0.24 electron equivalents and delivers 8 mAh/g capacity. In contrast, $Ag_{1.54}Mn_8O_{15.48}$ delivers 1.04 electron equivalents and 31 mAh/g. This is the first direct observation of hollandite with high
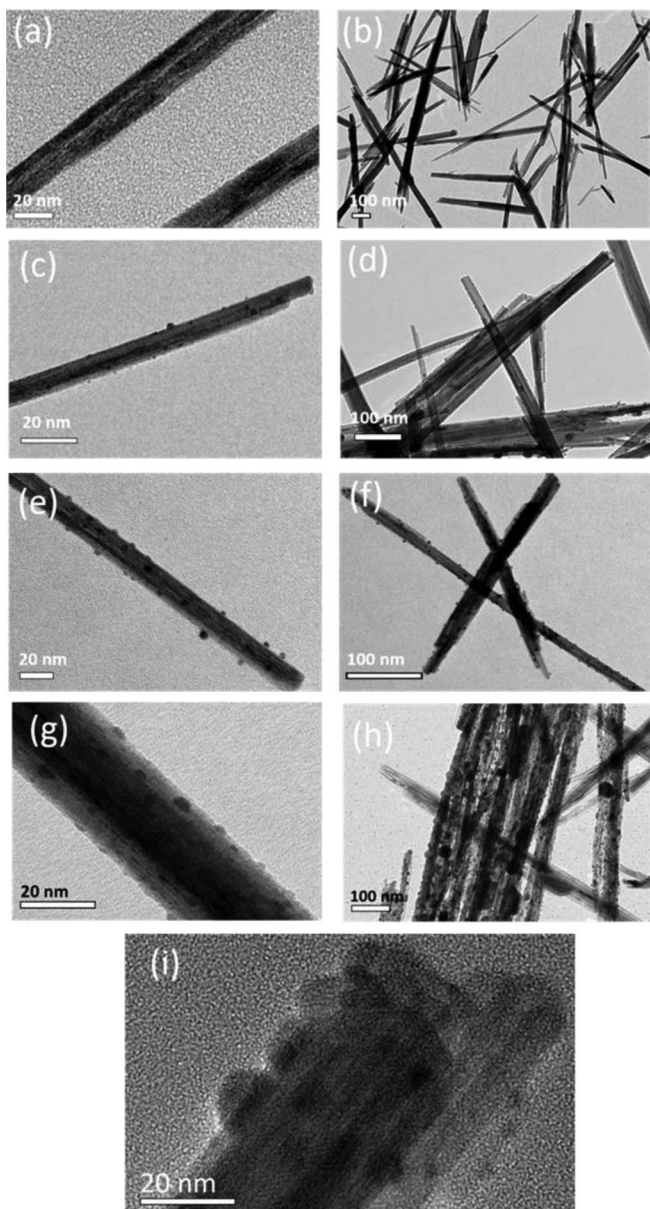
Figure 3. High and low magnification TEM images of (a) and (b) $Ag_{1.54}Mn_8O_{15.48}$, (c) and (d) $Ag_{1.54}Mn_8O_{15.48} \cdot 0.25\ Ag_2O$, (e) and (f) $Ag_{1.54}Mn_8O_{15.48} \cdot 0.63Ag_2O$, (g) and (h) $Ag_{1.54}Mn_8O_{15.48} \cdot 1.43Ag_2O$ (i) High resolution TEM for $Ag_{1.54}Mn_8O_{15.48} \cdot 1.43Ag_2O$.
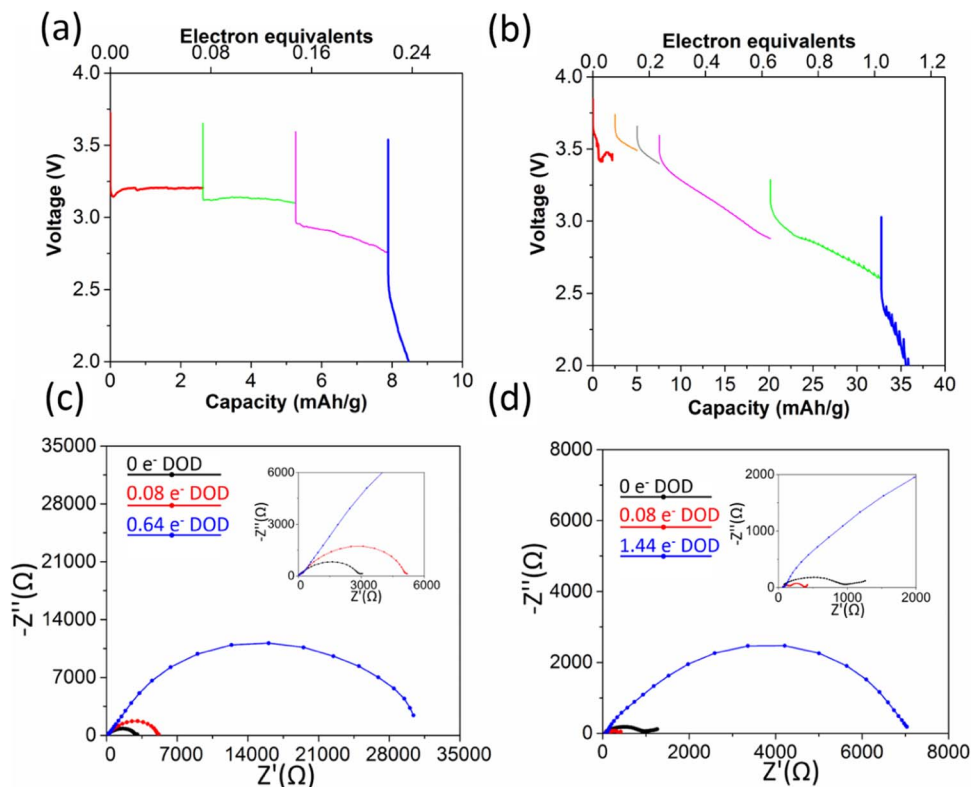

Figure 4. (a) Voltage of Li/Ag_2O electrochemical cells discharged under galvanostatic control (b) Nyquist plots of Ag_2O cells before and after the battery test, inset: Equivalent circuit used for mathematical fit.

Ag content delivering higher capacity during electrochemical reduction compared to low Ag content hollandite.[27] This observation may be attributed to limited electronic conductivity, as shown in the AC impedance of $Ag_{1.13}Mn_8O_{15.15}$ and $Ag_{1.54}Mn_8O_{15.48}$ before and after discharge in Figures 5c and 5d. The initial impedance is ~3000 Ω and ~1000 Ω for $Ag_{1.13}Mn_8O_{15.15}$ and $Ag_{1.54}Mn_8O_{15.48}$, respectively. Upon discharge to 0.08 electron equivalents the impedance for the $Ag_{1.13}Mn_8O_{15.15}$ cell increased to ~5000 Ω while the impedance for $Ag_{1.54}Mn_8O_{15.48}$ decreased to ~500 Ω. Further reduction led to increased impedance in both cases with a more significant increase for $Ag_{1.13}Mn_8O_{15.15}$ at a lower molar electron equivalent than $Ag_{1.54}Mn_8O_{15.48}$ (see Table III).

Lithium cells using $Ag_{1.13}Mn_8O_{15.15} \cdot 0.25Ag_2O$ or $Ag_{1.54}Mn_8O_{15.48} \cdot 0.25Ag_2O$ as cathodes showed sloping voltage profiles with discharge, Figures 6a and 6b. Above 2.2 V, $Ag_{1.54}Mn_8O_{15.48} \cdot 0.25Ag_2O$ delivered the higher capacity, 46 mAh/g, compared to 30 mAh/g for $Ag_{1.13}Mn_8O_{15.15} \cdot 0.25Ag_2O$, higher than

that of $Ag_{1.54}Mn_8O_{15.48}$ and $Ag_{1.13}Mn_8O_{15.15}$ (31 mAh/g and 8 mAh/g, respectively). The Nyquist plots for the cells are shown in Figures 6c and 6d. The initial impedance is ~500 Ω for both materials (Table III), which represents a substantial decrease relative to the uncoated silver hollandite. Notably, the impedance increases with discharge. For $Ag_{1.13}Mn_8O_{15.15} \cdot 0.63Ag_2O$ and $Ag_{1.54}Mn_8O_{15.48} \cdot 0.63Ag_2O$, (Figures 7a and 7b) the initial loaded voltage of 3.19 V and 3.23 V recovers to 3.23 V and 3.32 V within the first 0.01 electron equivalents of inserted Li+. With further discharge, the voltage profiles of both materials slope, and the $Ag_{1.13}Mn_8O_{15.15}$ structure now outperforms $Ag_{1.54}Mn_8O_{15.48}$, delivering ca. 90 vs. 65 mAh/g above 2.2 V. This correlates with an observed reduced impedance during initial discharge for $Ag_{1.13}Mn_8O_{15.15}$ (Figure 7c). We note both $Ag_{1.13}Mn_8O_{15.15} \cdot 0.63Ag_2O$ and $Ag_{1.54}Mn_8O_{15.48} \cdot 0.63Ag_2O$ showed an increase in impedance with continued discharge (Table III), further suggesting Mn reduction rather than continued formation of Ag^0.

The discharge profiles of $Ag_{1.54}Mn_8O_{15.48} \cdot 1.43Ag_2O$ and $Ag_{1.13}Mn_8O_{15.15} \cdot 1.43Ag_2O$ are shown in Figures 8a and 8b. Both curves showed sloping profiles, and above 2.2 V $Ag_{1.13}Mn_8O_{15.15}$ yielded higher capacity than $Ag_{1.54}Mn_8O_{15.48}$. Notably, above 1.5 V the capacity of the $Ag_{1.54}Mn_8O_{15.48} \cdot 1.43Ag_2O$ cell reaches 230 mAh/g, which is the highest value of all the cells discussed above. The high capacity can be attributed to significantly lower impedance at high levels of discharge (Table III), concurrent with the appearance of Ag metal by XRD (Figure 9).

A plot of energy density above 2.2 V vs. the Ag_2O content in the pure $Ag_xMn_8O_{16-y}$ materials and the $Ag_xMn_8O_{16-y} \cdot aAg_2O$ composites compares the electrochemistry of lower silver (x = 1.13) and higher (x = 1.54) intra-tunnel silver containing materials, Figure 10.
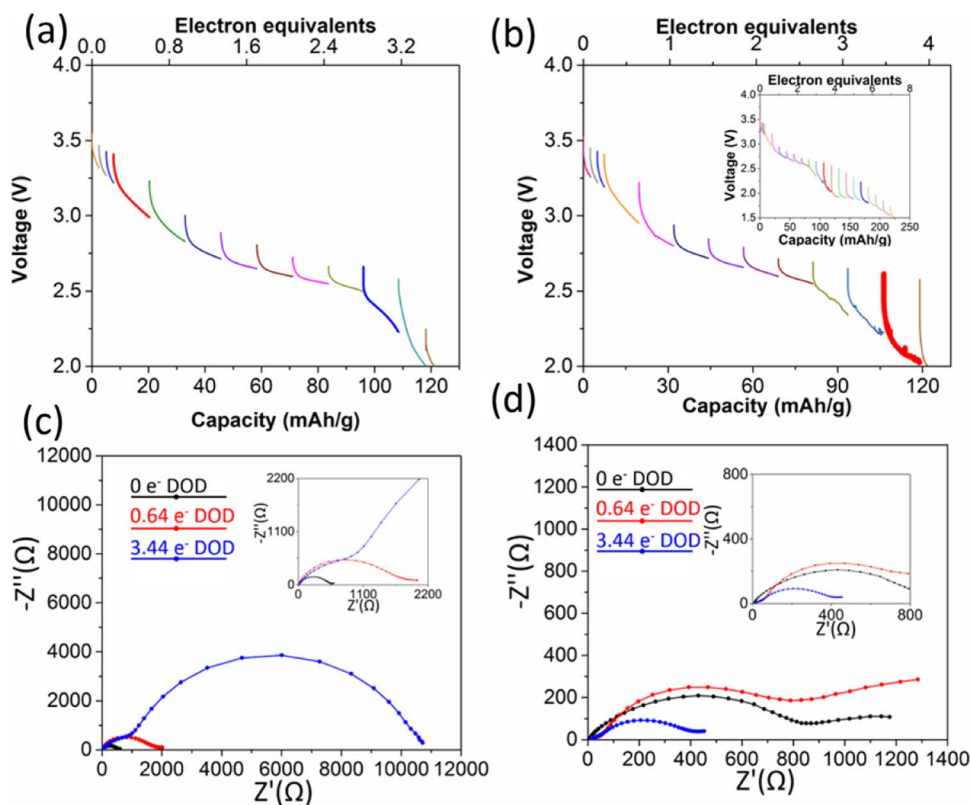
Figure 5. Voltage of (a) Li/Ag$_{1.13}$Mn$_8$O$_{15.15}$ and (b) Li/Ag$_{1.54}$Mn$_8$O$_{15.48}$ electrochemical cells discharged under galvanostatic control. Nyquist plots of (c)Ag$_{1.13}$Mn$_8$O$_{15.15}$ and (d) Ag$_{1.54}$Mn$_8$O$_{15.48}$ cells before and after the battery test.
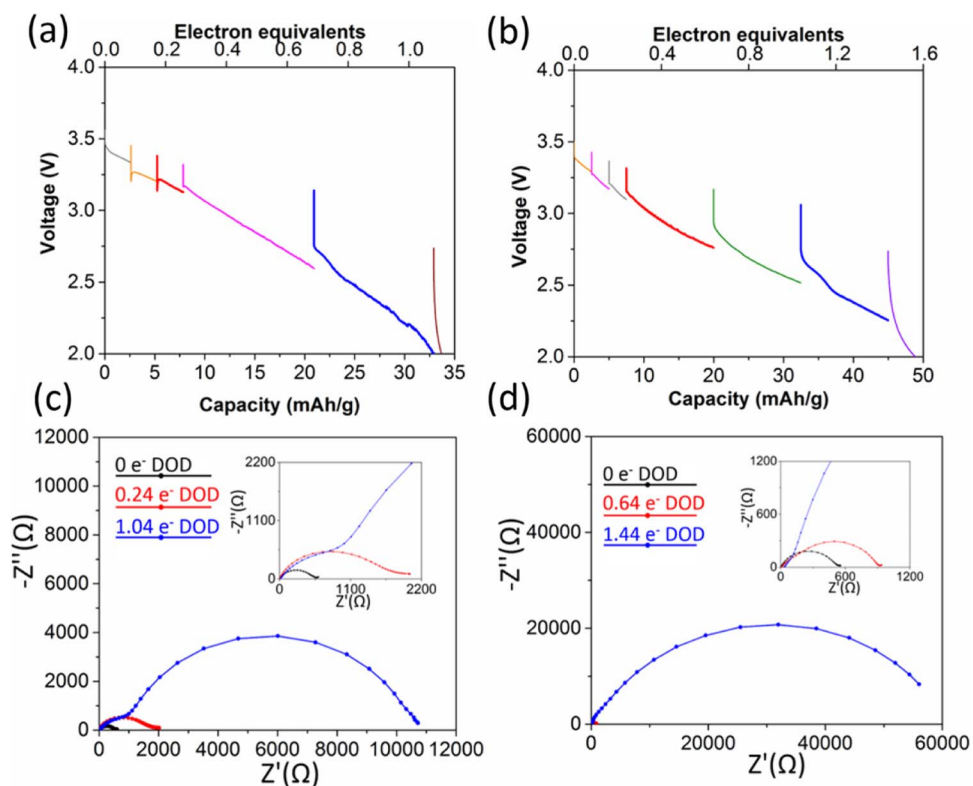
Figure 6. Voltage of (a) Li/Ag$_{1.13}$Mn$_8$O$_{15.15}$ · 0.25Ag$_2$O and (b) Li/Ag$_{1.54}$Mn$_8$O$_{15.48}$ · 0.25Ag$_2$O electrochemical cells discharged under galvanostatic control. Nyquist plots of (c) Ag$_{1.13}$Mn$_8$O$_{15.15}$ · 0.25Ag$_2$O and (d) Ag$_{1.54}$Mn$_8$O$_{15.48}$ · 0.25Ag$_2$O cells before and after the battery test.
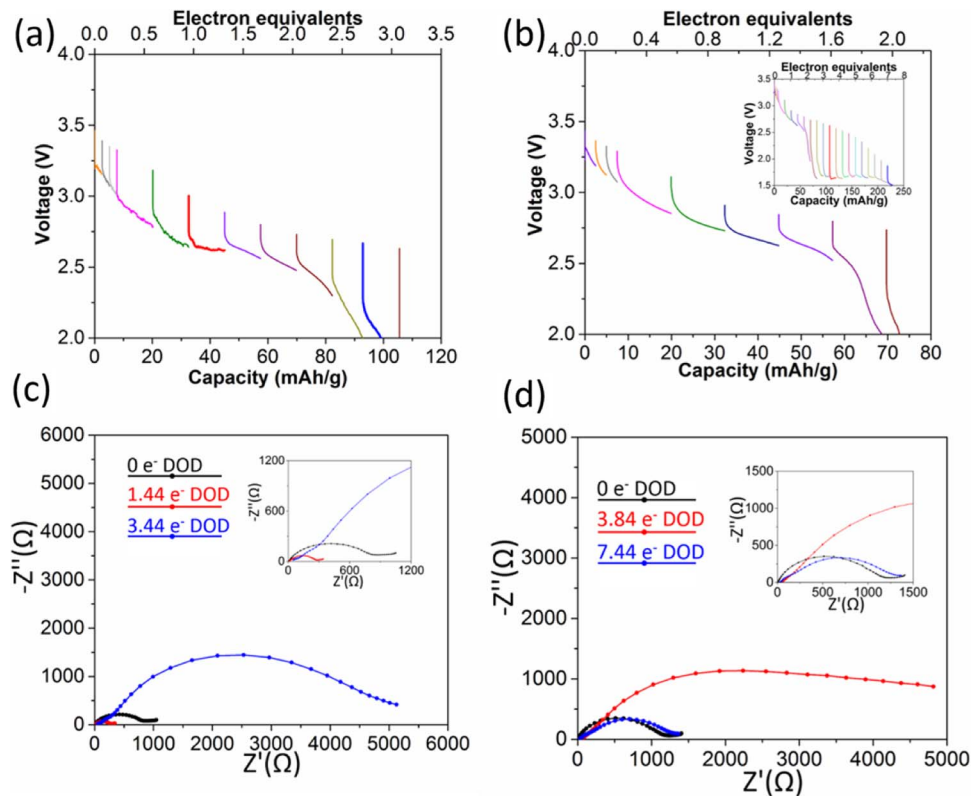
Figure 7. Voltage of (a) Li/Ag$_{1.13}$Mn$_8$O$_{15.15}$ · 0.63Ag$_2$O and (b) Li/Ag$_{1.54}$Mn$_8$O$_{15.48}$ · 0.63Ag$_2$O electrochemical cells discharged under galvanostatic control. Nyquist plots of (c) Ag$_{1.13}$Mn$_8$O$_{15.15}$ · 0.63Ag$_2$O and (d) Ag$_{1.54}$Mn$_8$O$_{15.48}$ · 0.63Ag$_2$O cells before and after the battery test.

Figure 8. Voltage of (a) Li/Ag$_{1.13}$Mn$_8$O$_{15.15}$ · 1.43Ag$_2$O and (b) Li/Ag$_{1.54}$Mn$_8$O$_{15.48}$ · 1.43Ag$_2$O electrochemical cells discharged under galvanotatic control. Nyquist plots of (c) Ag$_{1.13}$Mn$_8$O$_{15.15}$ · 1.43Ag$_2$O and (d) Ag$_{1.54}$Mn$_8$O$_{15.48}$ · 1.43Ag$_2$O cells before and after the battery test.

Table III. Results of fit of AC impedance data to resistance elements of equivalent circuit model shown in Figure 4b inset.

Materials	DOD	Rs (Ω) (error)	Rm+Rct (Ω)
Ag_2O	0 e$^-$	14 (3%)	3E5
	0.02 e$^-$	10 (1%)	503
	0.56 e$^-$	7 (1%)	176
$Ag_{1.13}Mn_8O_{15.15}$	0 e$^-$	4 (4%)	2717
	0.08 e$^-$	10 (2%)	5251
	0.64 e$^-$	11(4%)	30306
$Ag_{1.54}Mn_8O_{15.48}$	0 e$^-$	25 (18%)	975
	0.08 e$^-$	46 (16%)	465
	1.44 e$^-$	62 (5%)	7025
$Ag_{1.13}Mn_8O_{15.15} \cdot 0.25Ag_2O$	0 e$^-$	3 (1%)	450
	0.24 e$^-$	4 (2%)	1468
	1.04 e$^-$	11 (2%)	10923
$Ag_{1.54}Mn_8O_{15.48} \cdot 0.25Ag_2O$	0 e$^-$	4 (4%)	511
	0.64 e$^-$	10 (1%)	788
	1.44 e$^-$	37 (2%)	60655
$Ag_{1.13}Mn_8O_{15.15} \cdot 0.63Ag_2O$	0 e$^-$	5 (9%)	883
	1.44 e$^-$	9 (2%)	348
	3.44 e$^-$	3 (11%)	4891
$Ag_{1.54}Mn_8O_{15.48} \cdot 0.63Ag_2O$	0 e$^-$	5 (9%)	1266
	3.84 e$^-$	35 (4%)	4047
	7.44 e$^-$	27 (2%)	1344
$Ag_{1.13}Mn_8O_{15.15} \cdot 1.43Ag_2O$	0 e$^-$	9 (15%)	314
	0.64 e$^-$	2 (21%)	1954
	3.44 e$^-$	3 (11%)	10980
$Ag_{1.54}Mn_8O_{15.48} \cdot 1.43Ag_2O$	0 e$^-$	2 (56%)	1031
	3.84 e$^-$	7 (44%)	1001
	5.84 e$^-$	5 (47%)	386

For materials with no (a = 0) or low (a = 0.25) Ag_2O content, the higher intra-tunnel silver material (x = 1.54) exhibits higher energy density, which can be ascribed to 2–10x lower impedance values. At higher Ag_2O values (a = 0.63 or 1.43) the lower intra-tunnel silver material (x = 1.13) exhibits higher energy density as well as lower impedance. Thus, despite the lower amount of silver, Li$^+$ conduction becomes a more significant contributor to deliverable energy density once electron conduction is available. This trend generally holds for delivered capacity for the series of materials as well, Figure 10 inset.
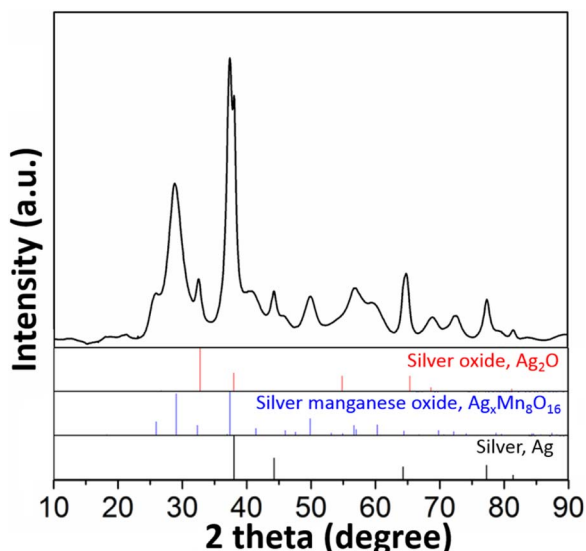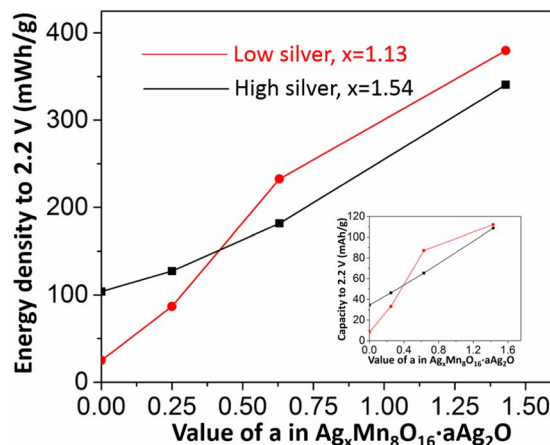
Figure 10. The relationship between Ag_2O content and the energy density above 2.2 V for two hollandites of different tunnel Ag concentration, inset: the relationship between Ag_2O content and the capacity.

Conclusions

We have shown that a coprecipitation method allows for coating silver oxide on silver hollandite nanorods, preparing $Ag_xMn_8O_{16-y} \cdot aAg_2O$ composites. XRD, FT-IR and TEM confirm the presence of Ag_2O on the surface of the as-synthesized samples. The ratio of $Ag_xMn_8O_{16-y}$ to Ag_2O in each sample was quantified using ICP-OES results. Electrochemical measurements under intermittent galvanostatic discharge and AC impedance indicate that the impedance of the $Ag_xMn_8O_{16-y} \cdot aAg_2O$ composites is lower than the pure $Ag_xMn_8O_{16-y}$. A capacity as high as 230 mAh/g was delivered by the $Ag_{1.54}Mn_8O_{15.48} \cdot 1.43Ag_2O$ composite. The quantity of Ag$^+$ in the tunnel correlates with increased capacity under conditions of limiting electron access where $Ag_{1.54}Mn_8O_{15.48}$ delivers higher capacity than $Ag_{1.13}Mn_8O_{15.15}$. For the Ag_2O containing composites, with low levels of Ag_2O (a = 0.25) $Ag_{1.54}Mn_8O_{15.48} \cdot 0.25Ag_2O$ delivers higher capacity than $Ag_{1.13}Mn_8O_{15.15} \cdot 0.25Ag_2O$. However, with higher levels of Ag_2O (a = 0.63 or 1.43) the $Ag_{1.13}Mn_8O_{15.15} \cdot aAg_2O$ composites deliver higher capacity. This study illustrates that Ag_2O coatings can significantly impact functional electrochemistry through contribution to reduced impedance and can lend insight into the structure/function relationships associated with electrochemistry in electron rich or electron limited environments.

References

1. J. E. Post, *Proc. Natl. Acad. Sci.*, **96**, 3447 (1999).
2. J. W. Gruner, *Am. Mineral.*, **28**, 497 (1943).
3. D. A. Tompsett and M. S. Islam, *Chemistry of Materials*, **25**, 2515 (2013).
4. C. Ling and F. Mizuno, *Chemistry of Materials*, **24**, 3943 (2012).
5. T. Ozawa, I. Suzuki, and H. Sato, *Journal of the Physical Society of Japan*, **75**, 014802 (2006).
6. J. Vicat, E. Fanchon, P. Strobel, and Q. D. Tran, *Acta Crystallogr, Sect. B: Struct. Sci.*, **B42**, 162 (1986).
7. T. S. Arthur, R. Zhang, C. Ling, P. A. Glans, X. Fan, J. Guo, and F. Mizuno, *ACS applied materials & interfaces*, **6**, 7004 (2014).
8. F. M. Chang and M. Jansen, *Angew. Chem., Int. Ed. Engl.*, **23** (1984).
9. E. Nicolas-Tolentina, Z.-R. Tian, H. Zhou, G. Xia, and S. L. Suib, *Chem. Mater.*, **11**, 1733 (1999).
10. M. Tsuji and S. Komarneni, *J. Mater. Res.*, **8**, 611 (1993).

Figure 9. XRD patterns of $Ag_{1.54}Mn_8O_{15.48} \cdot 1.43Ag_2O$ after discharging to 3.2 e$^-$.

11. L. Li and D. L. King, *Chem. Mater.*, **17**, 4335 (2005).
12. A. Dyer, M. Pillinger, J. Newton, R. Harjula, T. Moller, and S. Amin, *Chem. Mater.*, **12**, 3798 (2000).
13. K. J. Takeuchi, S. Z. Yau, M. C. Menard, A. C. Marschilok, and E. S. Takeuchi, *ACS applied materials & interfaces*, **4**, 5547 (2012).
14. K. J. Takeuchi, S. Z. Yau, A. Subramanian, A. C. Marschilok, and E. S. Takeuchi, *Journal of the Electrochemical Society*, **160**, A3090 (2013).
15. S. Zhu, A. C. Marschilok, C.-Y. Lee, E. S. Takeuchi, and K. J. Takeuchi, *Electrochemical and Solid-State Letters*, **13**, A98 (2010).
16. J. Huang, A. C. Marschilok, E. S. Takeuchi, and K. J. Takeuchi, *Chemistry of Materials*, **28**, 2191 (2016).
17. W. C. West, J. Soler, M. C. Smart, B. V. Ratnakumar, S. Firdosy, V. Ravi, M. S. Anderson, J. Hrbacek, E. S. Lee, and A. Manthiram, *Journal of The Electrochemical Society*, **158**, A883 (2011).
18. Y. Seok Jung, A. S. Cavanagh, Y. Yan, S. M. George, and A. Manthiram, *Journal of The Electrochemical Society*, **158**, A1298 (2011).
19. J. Liu, Q. Wang, B. Reeja-Jayan, and A. Manthiram, *Electrochemistry Communications*, **12**, 750 (2010).
20. M. Chen, L. L. Shao, H. B. Yang, Q. Y. Zhao, and Z. Y. Yuan, *Electrochimica Acta*, **168**, 59 (2015).
21. O. J. Kwon, Y. S. Jung, J. H. Kim, and S. M. Oh, *Journal of power sources*, **125**, 221 (2004).
22. M. He, Q. Sa, G. Liu, and Y. Wang, *ACS applied materials & interfaces*, **5**, 11152 (2013).
23. D. C. Giancoli, *Physics: Principles with Applications – Fourth Edition*, Prentice Hall, New Jersey, USA (1995).
24. X. Lin, K. Wu, L. Shao, M. Shui, X. Jiang, D. Wang, N. Long, Y. Ren, and J. Shu, *Journal of Alloys and Compounds*, **598**, 68 (2014).
25. A. C. Marschilok, K. J. Takeuchi, and E. S. Takeuchi, *Electrochemical and Solid-State Letters*, **12**, A5 (2009).
26. E. S. Takeuchi, A. C. Marschilok, K. Tanzil, E. S. Kozarsky, S. Zhu, and K. J. Takeuchi, *Chemistry of Materials*, **21**, 4934 (2009).
27. L. Wu, F. Xu, Y. Zhu, A. B. Brady, J. Huang, J. L. Durham, E. Dooryhee, A. C. Marschilok, E. S. Takeuchi, and K. J. Takeuchi, *ACS Nano*, **9**, 8430 (2015).
28. K. C. Kirshenbaum, D. C. Bock, Z. Zhong, A. C. Marschilok, K. J. Takeuchi, and E. S. Takeuchi, *J. Mater. Chem. A*, **3**, 18027 (2015).
29. L. Chen, H. Hua, Q. Yang, and C. Hu, *Applied Surface Science*, **327**, 62 (2015).
30. N. L. Yong, A. Ahmad, and A. W. Mohammad, *International journal of scientific&engineering reseach*, **4** (2013).
31. J. L. Durham, K. Kirshenbaum, E. S. Takeuchi, A. C. Marschilok, and K. J. Takeuchi, *Chemical communications*, **51**, 5120 (2015).
32. K. C. Kirshenbaum, D. C. Bock, Z. Zhong, A. C. Marschilok, K. J. Takeuchi, and E. S. Takeuchi, *Physical chemistry chemical physics : PCCP*, **16**, 9138 (2014).